

Ceramics International

[doi:10.1016/j.ceramint.2014.11.033](https://doi.org/10.1016/j.ceramint.2014.11.033)

Spark plasma sintering of graphene reinforced hydroxyapatite composites

Szilvia Klébert<sup>1\*</sup>, Csaba Balázsi<sup>2</sup>, Katalin Balázsi<sup>3</sup> Eszter Bódis<sup>1</sup>, Péter Fazekas<sup>1</sup>, Anna Mária Keszler<sup>1</sup>, János Szépvölgyi<sup>1</sup>, Zoltán Károly<sup>1</sup>

<sup>1</sup>Institute of Materials and Environmental Chemistry, Research Centre for Natural Sciences HAS, Magyar tudósok körútja 2, 1117, Budapest Hungary

<sup>2</sup>Institute for Materials Science and Technology, Bay Zoltán Nonprofit Ltd. for Applied Research, Fehérvári str. 130, 1116 Budapest, Hungary

<sup>3</sup>Institute for Technical Physics and Materials science, Research Centre for Natural Sciences, Hungarian Academy of Sciences, Konkoly-Thege M. str 29-33, 1121 Budapest, Hungary

\*Szilvia Klébert – [klebert.szilvia@ttk.mta.hu](mailto:klebert.szilvia@ttk.mta.hu), +36-1-3826 505

Csaba Balázsi – [csaba.balazsi@bayzoltan.hu](mailto:csaba.balazsi@bayzoltan.hu)

Katalin Balázsi – [balazsi.katalin@ttk.mta.hu](mailto:balazsi.katalin@ttk.mta.hu)

Eszter Bódis – [bodis.eszter@ttk.mta.hu](mailto:bodis.eszter@ttk.mta.hu)

Péter Fazekas – [fazekas.peter@ttk.mta.hu](mailto:fazekas.peter@ttk.mta.hu)

Anna Mária Keszler – [keszler.anna.maria@ttk.mta.hu](mailto:keszler.anna.maria@ttk.mta.hu)

János Szépvölgyi – [szepvolgyi.janos@ttk.mta.hu](mailto:szepvolgyi.janos@ttk.mta.hu)

Zoltán Károly – [karoly.zoltan@ttk.mta.hu](mailto:karoly.zoltan@ttk.mta.hu)

## Abstract

Hydroxyapatite (prepared from eggshell) / graphene (HAP/GNPs) composites were prepared by spark plasma sintering (SPS). Pure HAP does not have good mechanical properties so it is necessary to associate with some materials, which contribute acceptable strength properties. Sintering was carried out at various temperatures (700°C and 900°C) and holding times (5 and 10 min). Using SPS is explained by the rapid process time to avoid HAP decomposition. Mechanical and structural properties of the sintered bodies were studied with different methods. The highest relative density ~ 96% was obtained at 700°C sintering temperature independently on holding time. Composite with highest mechanical properties (hardness ~ 4 GPa, 3-point bending strength ~119 MPa) consisted of HAP elongated grains with average length of 300 nm. The GNPs were agglomerated and located on grain boundaries closed to porosities. The structural observation confirmed increased fraction of hexagonal shaped grains, and poorer mechanical properties with increased sintering time and temperature.

**Keywords:** SPS, Hydroxyapatite, graphene, composite, hardness

## 1. Introduction

Implant biomaterials brought into direct contact with body tissue without any intermediate layer. Biomaterials may be divided into three main groups; plastics, metals or alloys and ceramics [1, 2]. The most promising bioceramic material is a hydroxyapatite (HAP,  $\text{Ca}_{10}(\text{PO}_4)_6(\text{OH})_2$ ). It is a most used implant for tissue implantation due to its similarity with apatite in human skeletal system, bone and teeth in terms of the chemical composition (Ca/P ratio of 1.67) and crystal structure [3]. HAP in different forms (powder, fiber, sintered) exhibited the excellent biocompatibility [4,5]. Sintered HAP may be an ideal candidate for orthopaedic and dental implants. The sintered HAP body showed lower mechanical properties as poor fatigue resistance, low toughness and flexural strength, which restrict its use as a major load bearing parts in the body [6]. Moreover, its chemical stability is limited to tri-and tetracalcium phosphates when exposed to prolonged heat during processing [7-9]. One of route to increasing the poor mechanical properties of sintered HAP is a development of nanosized HAP [10,11]. The nanosized HAP can improve the sintering kinetics due to higher surface area and hence improved mechanical properties [12]. Other possible ways to overcome these mechanical limitations include the incorporation of a second reinforcement phase in the HAP matrix and lowering the sintering temperature to avoid chemical decomposition. Among reinforcing fillers glass, alumina, or various carbon nanostructures, such as carbon nanotubes or graphene nanoplatelets have been investigated [13-17]. Graphene nanoplatelets (GNPs) formed by several layers of graphene with a thickness of up to 50 nm [18]. The superior properties of graphene or GNPs have already been utilized as filler additive to polymers [19-21] or ceramics [22]. So far only a few reports have been published on the use of graphene additive to

1 improve the mechanical properties of hydroxyapatite ceramics [23]. Zhao et al. [24]  
2 prepared graphene platelet/biphasic calcium phosphate composites by hot pressing. He  
3 reported a considerable improvement in terms of mechanical properties like bending  
4 strength and fracture toughness using 1.5 wt% GNPs.  
5

6  
7  
8  
9  
10 Contrary to other traditional sintering techniques in SPS the sample is directly heated by  
11 the applied electric current which results in quite fast and effective heating [25,26].  
12  
13 Even though the precise mechanism of sintering by pulsed electric current has not been  
14 clearly understood yet, its beneficial features are undeniable. This includes the clean  
15 interphases, the restricted grain growth because of lower temperature and shorter  
16 holding time, which eventually allows the production of nanostructured ceramics [13].  
17  
18 In this work, graphene nanoplatelets were used for reinforcing nanosized HAP and the  
19 densification processes were carried out by SPS method. The structural and mechanical  
20 properties of the HAP / GNPs composites have been studied. The effects of applied  
21 sintering temperature (700°C, 900°C) and holding time (5 min, 10 min) on the  
22 mechanical properties and the structure of the composites are discussed.  
23  
24  
25  
26  
27  
28  
29  
30  
31  
32  
33  
34  
35  
36  
37  
38  
39

## 40 2. Experimental Procedure

### 41 2.1 Starting mixture

42  
43  
44  
45  
46  
47 The starting powders used in these experiments were HAP powder and graphene. HAP  
48 preparation from eggshell and orthophosphoric acid in the laboratory was described  
49 earlier [27]. The as-prepared HAP powder is of 66 nm in size. The mean size was  
50 calculated from the measured specific surface area ( $29 \text{ m}^2 \cdot \text{g}^{-1}$ ) of the HAP powder by 7  
51 point BET method using Autosorb 1C apparatus. However, because of the high surface  
52  
53  
54  
55  
56  
57  
58  
59  
60  
61  
62  
63  
64  
65

activity, HAP grains formed 5-20  $\mu\text{m}$  size agglomerates. Multilayer graphene (MLG) or graphene nanoplatelets (GNPs) was prepared by milling synthetic graphite (Aldrich) in ethanol using a highly efficient attritor mill (Union Process, type 01-HD/HDDM) equipped with zirconia agitator delta discs and zirconia grinding media in a 750 ml silicon nitride tank. The milling process has been performed with high rotation speed, 4000 rpm until 10 h. The milled product was dried and sieved with a filter with a mesh size of 325. According to analysis the mean thickness of the crystallites was 13.7 nm, which is equivalent to 40 graphene layers [28,29]. HAP powder and GNPs were mixed in a 98 to 2 wt% ratio and milled in a high efficient attritor mill equipped with zirconia agitator discs, zirconia grinding balls and zirconia tank (750 mL). This milling process has been performed in ethanol with high rotation speed (4000 rpm) for 2 hours, then the slurry was dried and sieved.

## 2.2 Sintering

The as-obtained mixtures were then sintered to discs of 3 cm in diameter and 5 mm in thickness by spark plasma sintering machine (HD P5, FCT GmbH). Composites with different sintering temperatures (700°C and 900°C) and holding times (5 and 10 minute) were prepared (Table 1.) The heating rate was 100°C/min up to 700°C and from 700 to 900°C it was decreased to 50°C/min for fearing of abrupt gas accumulation. Temperature was continuously measured by thermocouples inserted to the graphite die. A chamber pressure of 1 mbar was maintained during consolidation. The powders were uniaxially compressed throughout the sintering process with 50 MPa. Linear shrinkage

of the powder compacts was monitored on line by measuring the relative displacement of the graphite punch.

### 2.3 Analytical techniques

Densities of sintered bodies were measured using Archimedes' principle immersion method, both apparent and bulk densities were determined. Theoretical density was calculated from data of starting materials (for HAP: 3.16 g/cm<sup>3</sup>, for GNPs: 2.25 g/cm<sup>3</sup> [30]). X-ray diffraction (XRD) measurements were performed on a Siemens D5000 diffractometer using CuK $\alpha$ 1 radiation. Diffractograms were obtained in a step scanning mode  $20^{\circ} \leq 2\theta \leq 65^{\circ}$ . Three point bending strength measurements were carried out by AMMRC 85-21 standard procedure (U.S. army standard test method for flexural strength of high performance ceramics at ambient temperature) using an INSTRON 5966 instrument on rectangular specimens with dimensions of 28 mm  $\times$  5 mm  $\times$  2.5 mm. Each specimen was grounded and the edges were chamfered. The obtained value represents the results of three parallel measurements. Microhardness of composites was measured after polishing by Leitz Miniload 2 microhardness tester with an applied load of 4.903 N and a holding time of 27 s. The morphology of synthesized bodies was characterized by scanning electron microscopy (SEM, Zeiss type DSM 982 GEMINI with a heated field emission tungsten cathode).

Sample	HAP	GNPs	SPS condition		
	wt%	wt%	Temperature	Pressure	Time

			[°C]	[MPa]	[min]
HG-5-7	98	2	700	30	5
HG-5-9			900		
HG-10-7			700		10
HG-10-9			900		

Table 1. SPS conditions during HAP composites preparation.

### 3. Results and Discussion

#### 3.1 Thermodynamic calculation

During sintering the HAP composites are exposed to high temperature so chemical reaction may also occur beside consolidation. As graphene layers were incorporated in the mixture and the die itself is made of graphite reduction may also take place between components. In order to predict the possible reactions thermodynamic calculation was carried out by code FACTSAGE, which determines the thermodynamically most stable phases and their relative amounts at a given temperature and pressure by Gibbs energy minimization.



Figure 1. Chemical equilibrium diagram for the HAP/GNPs system assuming a 2:0.5 HAP:C molar ratio

The results of the theoretical calculations (Figure 1.) gave different values for the decomposition of HAP in the presence of carbon and without carbon. Decomposition of pure HAP occurs at around 1400°C, which is in line with literature and is confirmed by thermogravimetric measurements [31]. In the presence of carbon decomposition temperature drops a little bit, however, HAP is chemically stable even up to 1000°C. According to Cihlár [32] HAP decomposition takes place in two steps: first is at around 900 °C where the water leaves the system leading to oxyapatite, and the second one occurs at above 1300°C resulting in calcium phosphates and calcium oxide. Considerable development of CO, CO<sub>2</sub> and H<sub>2</sub> gases is also expected, which might be also of interest in technical the point of view as sintering is carried out in a closed system. To avoid the undesirable formation of calcium phosphates, which impair the mechanical properties of HAP the SPS sintering experiments were performed temperature below 1000°C, at 700°C and 900°C, respectively.

### 3.2 SPS

Figure 2. The sintering curves on 700°C (a) and 900°C (b) in the function of time

Figures 2.a-b shows the sintering curves of the experiments conducted at 700 and 900°C for 10 minutes including the temperature, the shrinkage as well as the rate of shrinkage

1 in the function of treatment time. From the latter curve it is apparent that sintering starts  
2  
3 below the max sintering temperature at around 600°C. The peaks under this temperature  
4  
5 refer to the compaction on the effect of the increasing compression. The two peaks of  
6  
7 the rate of shrinkage above 500°C on Figure 2.b is due to the change in the heating rate  
8  
9 above 700°C. In this way the rate slowed down than increased again at reaching the  
10  
11 maximum temperature. Comparing the Figures show that the increased temperature  
12  
13 gave rise to further shrinkage that implies to better consolidation. However, the  
14  
15 prolonged sintering time from 5 to 10 minutes apparently does not result in further  
16  
17 shrinkage.  
18  
19  
20  
21  
22  
23  
24

25 On Figure 3 crystalline phases of the starting mixture and the sintered product are  
26  
27 compared. The absence of calcium phosphates on the XRD pattern of the sintered body  
28  
29 indicates that decomposition of HAP did not take place even at 900°C. The presence of  
30  
31 crystalline carbon in all XRD patterns, presumably in the form of graphene, confirms  
32  
33 that carbon did not react with other oxide component. The characteristic peaks of  
34  
35 CaCO<sub>3</sub> could be detected in minor intensity in all samples. Even though CaCO<sub>3</sub> is not  
36  
37 stable above 860 °C at atmospheric pressure, probably due to the applied uniaxial  
38  
39 pressure during SPS it did not decompose or at least not completely even at 900°C. The  
40  
41 main reason for the minor presence of CaCO<sub>3</sub> in the starting mixture is the preparation  
42  
43 method of HAP powder since it was synthesized from a biogenic material, eggshell as  
44  
45 detailed in [33].  
46  
47  
48  
49  
50  
51  
52  
53  
54

55 Figure 3. XRD patterns of the sintered bodies and the starting HAP powder  
56  
57  
58  
59  
60  
61  
62  
63  
64  
65

Sample	Composition of the synthesized powders (wt%) by XRD*			Relative density [%]	HV [GPa]	3 point bending strength [MPa]
	HAP	CaCO <sub>3</sub>	C			
HG-5-7	92	6	2	95.65	4 ± 0.5	119 ± 4.9
HG-10-7	92	6	2	95.88	3.5 ± 0.6	100 ± 4.8
HG-5-9	94	4	2	89.12	2.2 ± 0.4	84 ± 6.1
HG-10-9	94	4	2	87.44	2 ± 0.4	91 ± 5.2

Table 2. Characteristics and properties of the sintered samples

In Table 2. relative densities and other mechanical properties of particular tests obtained after sintering are listed. Density values show an interesting trend. Usually higher sintering temperature and longer sintering time are accompanied with higher density values. It could be anticipated also from the sintering curves, too. In contrast, samples prepared at 700 °C (HG-5-7 and HG-10-7) possess much higher theoretical density of ca. 96% than samples (HG-5-9 and HG-10-9) heat treated at 900°C. There are, however, only minor changes in the density values because of the prolonged holding time that is in accord to the sintering curves. The incomplete consolidation are usually attributed to pores remained inside the sample. Applying longer holding time some of the pores

could be eliminated that explains the slightly higher density of the sample HG-5-10, although it was not high. Again, against our expectations the density of HG-9-10 decreased on longer heating. One reason of the remaining porosity could be the presence of graphene layers. Increased numbers of pores was reported for other graphene incorporated ceramic composites [34], too. It was mainly attributed to the clustering of the graphene layers. The higher amount of pores at the higher sintering temperature, however, implies other sources of pore formation that occurs with increasing temperature. This suggests the decomposition of  $\text{CaCO}_3$  at higher temperature that result in  $\text{CO}_2$ . Alternatively, reaction may occur between the carbon and HAP. This is, however, should be excluded by the thermodynamics calculations. In addition, it is not confirmed by XRD results, either.

The relative densities and other mechanical properties of HAP samples obtained after sintering are listed in Table 2. Density values show an interesting trend. The higher relative densities were obtained in the case of  $700^\circ\text{C}$  sintering temperature compared with  $900^\circ\text{C}$ . The sintering time did not have discernible effect to the mechanical properties. One reason of the remaining porosity could be the presence of graphene layers. Increased numbers of pores was reported for other graphene incorporated ceramic composites [34], too. It was mainly attributed to the clustering of the graphene layers. The higher amount of pores at the higher sintering temperature, however, implies other sources of pore formation that occurs with increasing temperature. This suggests the decomposition of  $\text{CaCO}_3$  at higher temperature that result in  $\text{CO}_2$ . Alternatively, reaction may occur between the carbon and HAP. This fact should be excluded by the thermodynamics calculations. In addition, it is not confirmed by XRD results, either.

Mechanical properties including hardness and bending strength follow a similar trend as relative density (Table 2.). Higher values were achieved applying lower sintering temperature. This tendency is probably also related to porosity of the HAP/graphene samples.

The influence of 2 wt% graphene addition to the mechanical changes was observed. The hardness of pure HAP sintered at 600°C showed  $3.9 \pm 0.2$  GPa and 3 point bending strength was  $58 \pm 5$  MPa from our previous work [35]. This fact proves that the addition of graphene may the positive effect of mechanical properties of composite. The SEM investigations of HAP/graphene composites were shown in Fig. 4.

Figure 4. SEM images of HAP/graphene composites sintered at different parameters. a) 700°C and 5 min, b) 900°C and 5 min, c) 700°C and 10 min, d) 900°C and 10 min.

HAP / graphene composites sintered at lower sintering time (5 min) consisted of HAP elongated grains with average length of 300 nm. The GNPs were agglomerated and located on grain boundaries closed to porosities (Fig. 4a). The increasing of sintering time caused the change of main part of grain's morphology from elongated to polycrystalline form. The average length of grains doubled. The few micrometer GNPs were located between HAP grains (Fig. 4b).

Increasing of sintering temperature from 700°C to 900°C resulted in morphological change and decreased HAP grain size. The average size of polygonal HAP grains was around 200 – 250 nm. In this case, the 500 nm size GNPs were observed between HAP polygons (Fig. 4c).

The 900°C and 10 min sintering time resulted in HAP crystals of 800 nm – 1 µm length and 250 nm width. The GNPs plates were destructed to few tens nanometer size (Fig. 4d). Only in this case, no agglomeration of GNPs was observed.

The SEM observation confirmed increased fraction of hexagonal shaped grains with longer sintering time and higher temperature. Champion et al. claimed that grain growth during either pressureless sintering or SPS is significant only above 95% of theoretical density [25]. This fact also confirms that the lower values of theoretical density of the samples sintered at 900°C must be due to pores generated at that higher temperature probably by the decomposition of CaCO<sub>3</sub>. Nakahira et al. [36] and Watanabe et al. [37] showed that SPS at high temperatures leads to the selective growth of c-axis of HAP crystals, resulting in coarse acicular grains that tend to lie in planes perpendicular to the direction of the applied compressive stress. Similar microstructure developed in silicon nitride ceramics during SPS, Shen Z. et al. [38] studied the formation of elongated grains and their effect on toughness. They concluded that the mechanism of grain growth during SPS, named 'dynamical ripening' is different from the Ostwald ripening.

#### 4. Conclusions

In this work graphene nanoplatelet reinforced (2 wt%) hydroxyapatite bioceramics were prepared by spark plasma sintering. Low sintering temperatures (700 and 900 °C) and short holding times (5 and 10 min) were applied to avoid HAP decomposition and possible oxidation of the graphene platelets. The main findings were, as follows:

- SPS treatment of a HAP/2 wt% GNPs composite proved to be superior in terms of mechanical properties over pure sintered HAP items.

1 • Best combination of the mechanical properties were obtained at as lower  
2  
3 sintering temperature as 700 °C using 5 min sintering time with bending strength of 119  
4  
5 MPa and hardness value of 4 GPa. These values decreased at higher sintering  
6  
7 temperature (900°C) due to the increased porosity, which can be attributed to the  
8  
9 decomposition of the  $\text{CaCO}_3$  presented in minor amount in the starting powder as  
10  
11 impurities.  
12  
13

14 • At higher sintering temperature the amount of the hexagonal shaped grains  
15  
16 significantly increased, although their effect on the mechanical properties could not be  
17  
18 noticed.  
19  
20

21 The authors believe that even better properties could be achieved using other,  $\text{CaCO}_3$   
22  
23 free HAP as starting material and improving the dispersion method of graphene to  
24  
25 prevent its clustering in the matrix.  
26  
27  
28  
29  
30  
31

## 32 Acknowledgement

33  
34 The authors thanks to Dr. Gergely Gréta, Varga Viktor and Illés Levente from MTA  
35  
36 TTK MFA Budapest for powder sample preparation and SEM investigation. The  
37  
38 authors also kindly acknowledge the financial support of the National Office for  
39  
40 Research and Technology (REG-KM-09-1-2009-0005) and also to OTKA grant No.  
41  
42 105355 projects.  
43  
44  
45  
46  
47  
48  
49

## 50 References

51  
52 [1] R.B. Heimann, Classic and Advanced Ceramics – From Fundamentals to  
53  
54 Applications, Wiley, Weinheim, 2010.  
55  
56  
57  
58  
59  
60  
61  
62  
63  
64  
65

- [2] Z. Li, M.J. Kawashita, Current progress in inorganic artificial biomaterials, *Artif. Organs.* 14 (2011) 163-170.
- [3] T. Kokubo, *Bioceramics and their Clinical Applications*, Woodhead publishing Ltd., Cambridge, 2008.
- [4] S.V. Dorozhkin, Bioceramics of calcium orthophosphates, *Biomaterials* 31 (2010) 1465-1485.
- [5] S. Kalmodia, S. Goenka, T. Laha, D. Lahiri, B. Basu, K. Balani Microstructure, mechanical properties, and *in vitro* biocompatibility of spark plasma sintered hydroxyapatite–aluminum oxide–carbon nanotube composite *Mater. Sci. Eng. C Mater. Biol. Appl.* 30 (2006) 1162-1169.
- [6] D. Bellucci, A. Sola, M. Gazzarri, F. Chiellini, V. Cannillo A new hydroxyapatite-based biocomposite for bone replacement *Mater. Sci. Eng. C Mater. Biol. Appl.* (2013) 33 1091-1101.
- [7] Y. Liu, Z. Shen, Dehydroxylation of hydroxyapatite in dense bulk ceramics sintered by spark plasma sintering, *J. Eur. Ceram. Soc.* 32 (2012) 2691-2696.
- [8] Y.W. Gu, N.H. Loh, K.A. Khor, S.B. Tor, P. Cheang, Spark plasma sintering of hydroxyapatite powders, *Biomaterials* 23 (2002) 37-43.
- [9] A.C. Tas, Synthesis of biomimetic Ca-hydroxyapatite powders at 37 degrees C in synthetic body fluids, *Biomaterials* 21 (2000) 1429-1438.
- [10] W. Que, K.A. Khor, J.L. Xu, L.G. Yu, Hydroxyapatite/titania nanocomposites derived by combining high-energy ball milling with spark plasma sintering processes, *J. Eur. Ceram. Soc.* 28 (2008) 3083-3090.
- [11] D. Grossin, S. Rollin-Martinet, C. Estournès, F. Rossignol, E. Champion, C. Combes, C. Rey, C. Geoffroy, C. Drouet, Biomimetic apatite sintered at very low



temperature by spark plasma sintering: Physico-chemistry and microstructure aspects, *Acta Biomater.* 6 (2010) 577-585.

[12] S. Bose, S.K. Saha, Synthesis of hydroxyapatite nanopowders via sucrose-templated sol-gel method, *J. Am. Ceram. Soc.* 86 (2003) 1055-1057.

[13] W. Wang, Y. Zhu, F. Watari, S. Liao, A. Yokoyama, M. Omori, H. Ai, F. Cui, Carbon nanotubes/hydroxyapatite nanocomposites fabricated by spark plasma sintering for bonegraft applications, *Appl. Surf. Sci.* 262 (2012) 194-199.

[14] J.D. Santos, J.C. Knowles, R.L. Reis, F.J. Monteiro, G.W. Hastings, Microstructural Characterization of Glass-Reinforced Hydroxyapatite Composites, *Biomaterials* 15 (1994) 5-10.

[15] Y. Zhang, S. Tan, Y. Yin, C-fibre reinforced hydroxyapatite bioceramics, *Ceram. Int.* 29 (2003) 113-116.

[16] C. Kealley, M. Elcombe, A. Riessen, B. Ben-Nissan, Development of carbon nanotube-reinforced hydroxyapatite bioceramics, *Physica B Condens. Matter.* 385–386 (2006) 496-498.

[17] H. Ji, P.M. Marquis, Preparation and Characterization of  $\text{Al}_2\text{O}_3$  Reinforced Hydroxyapatite, *Biomaterials* 13 (1992) 744-748.

[18] J. Dusza, J. Morgiel, A. Duszová, L. Kvetková, M. Nosko, P. Kun, Cs. Balázsi, Microstructure and fracture toughness of  $\text{Si}_3\text{N}_4$  + graphene platelet composites, *J. Eur. Ceram. Soc.* 32 (2012) 3389-3397.

[19] S.A. Goldstein, The Mechanical Properties of Trabecular Bone - Dependence on Anatomic Location and Function, *J. Biomech.* 20 (1987) 1055-1061.

[20] T. Kuilla, S. Bhadra, D. Yao, N.H. Kim, S. Bose, J.H. Lee, Recent advances in graphene based polymer composites, *Prog. Polym. Sci.* 35 (2010) 1350-1375.

- [21] J.R. Potts, D.R. Dreyer, C.W. Bielawski, R.S. Ruoff, Graphene-based polymer nanocomposites, *Polym.* 52 (2011) 5-25.
- [22] A. Nieto, D. Lahiri, A. Agarwal, Nanodynamic mechanical behavior of graphene nanoplatelet-reinforced tantalum carbide, *Scr. Mater.* 69 (2013) 678-681.
- [23] J. Zhu, H.M. Wong, K.W.K. Yeung S.C. Tjong, (2011) Spark Plasma Sintered Hydroxyapatite/Graphite Nanosheet and Hydroxyapatite/Multiwalled Carbon Nanotube Composites: Mechanical and in Vitro Cellular Properties, *Adv. Eng. Mater.* 13 336-341.
- [24] Y. Zhao, K. Sun, W.L. Wang, Y. X. Wang, X. L. Sun, Y. J. Liang, X. N. Sun, P. F. Chui, Microstructure and anisotropic mechanical properties of graphene nanoplatelet toughened biphasic calcium phosphate composite, *Cer. Int.* 39 (2013) 7627-7634.
- [25] E. Champion, Sintering of calcium phosphate bioceramics, *Acta Biomater.* 9 (2013) 5855-5875.
- [26] D. Lahiri, V. Singh, A.K. Keshri, S. Seal, A. Agarwal, Carbon nanotube toughened hydroxyapatite by spark plasma sintering: Microstructural evolution and multiscale tribological properties, *Carbon* 48 (2010) 3103-3120.
- [27] Cs. Balázs, F. Wéber, Zs. Kövér, E. Horvath, Cs. Nemeth, Preparation of calcium-phosphate bioceramics from natural resources, *J. Eur. Ceram. Soc.* 27 (2007) 1601-1606.
- [28] L. Kvetková, A. Duszová, M. Kasiarová, F. Dorcáková, J. Dusza, Cs. Balázs, Influence of processing on fracture toughness of Si<sub>3</sub>N<sub>4</sub> + graphene platelet composites, *J. Eur. Ceram. Soc.* 33 (2013) 2299-2304.
- [29] P. Kun, F. Wéber, Cs. Balázs, Preparation and examination of multilayer graphene nanosheets by exfoliation of graphite in high efficient attritor mill, *Cent. Eur. J. Chem.* 9 (2011) 47-51.

- [30] M.I. Kay, R.A. Young, A.S. Posner, Crystal Structure of Hydroxyapatite, *Nature* 204:(1964) 1050-1052.
- [31] C.J. Liao, F.H. Lin, K.S. Chen, J.S. Sun, Thermal decomposition and reconstitution of hydroxyapatite in air atmosphere, *Biomaterials* 20 (1999) 1807-1813.
- [32] J. Cihlár, A. Buchal, M. Trunec, Kinetics of thermal decomposition of hydroxyapatite bioceramics, *J. Mat. Sci.* 34 (1999) 6121-6131.
- [33] G. Gergely, F. Wéber, I. Lukács, L. Illes, A.L. Toth, Z.E. Horvath, J. Mihaly, Cs. Balazsi, Nano-hydroxyapatite preparation from biogenic raw materials, *Cent. Eur. J. Chem.* 8 (2010) 375-381.
- [34] L. Kvetkova, A. Duszova, P. Hvizdos, J. Dusza, P. Kun, C. Balazsi, Fracture toughness and toughening mechanisms in graphene platelet reinforced Si<sub>3</sub>N<sub>4</sub> composites, *Scr. Mater.* 66 (2012) 793-796.
- [35] G. Gergely, C.F. Sahin, G. Göller, O. Yücel, Cs. Balázs, Microstructural and mechanical investigation of hydroxyapatite-zirconia nanocomposites prepared by spark plasma sintering, *J. Eur. Ceram. Soc.* 33 (2013) 2313-2319.
- [36] A. Nakahira, M. Tamai, K. Eguchi, S. Nakamura, K. Yamashita, Preparation and evaluation of dense hydroxyapatite by PECS method, *Key. Eng. Mat.* 240-242 (2003) 551-554.
- [37] Y. Watanabe, T. Ikoma, A. Monkawa, Y. Suetsugu, H. Yamada, J. Tanaka, Fabrication of transparent hydroxyapatite sintered body with high crystal orientation by pulse electric current sintering, *J. Am. Ceram. Soc.* 88 (2005) 243-245.
- [38] Z. Shen, Z. Zhao, H. Peng, M. Nygren, Formation of tough interlocking microstructures in silicon nitride ceramics by dynamic ripening, *Nature* 417 (2002) 266-269.

Figure1

[Click here to download high resolution image](#)

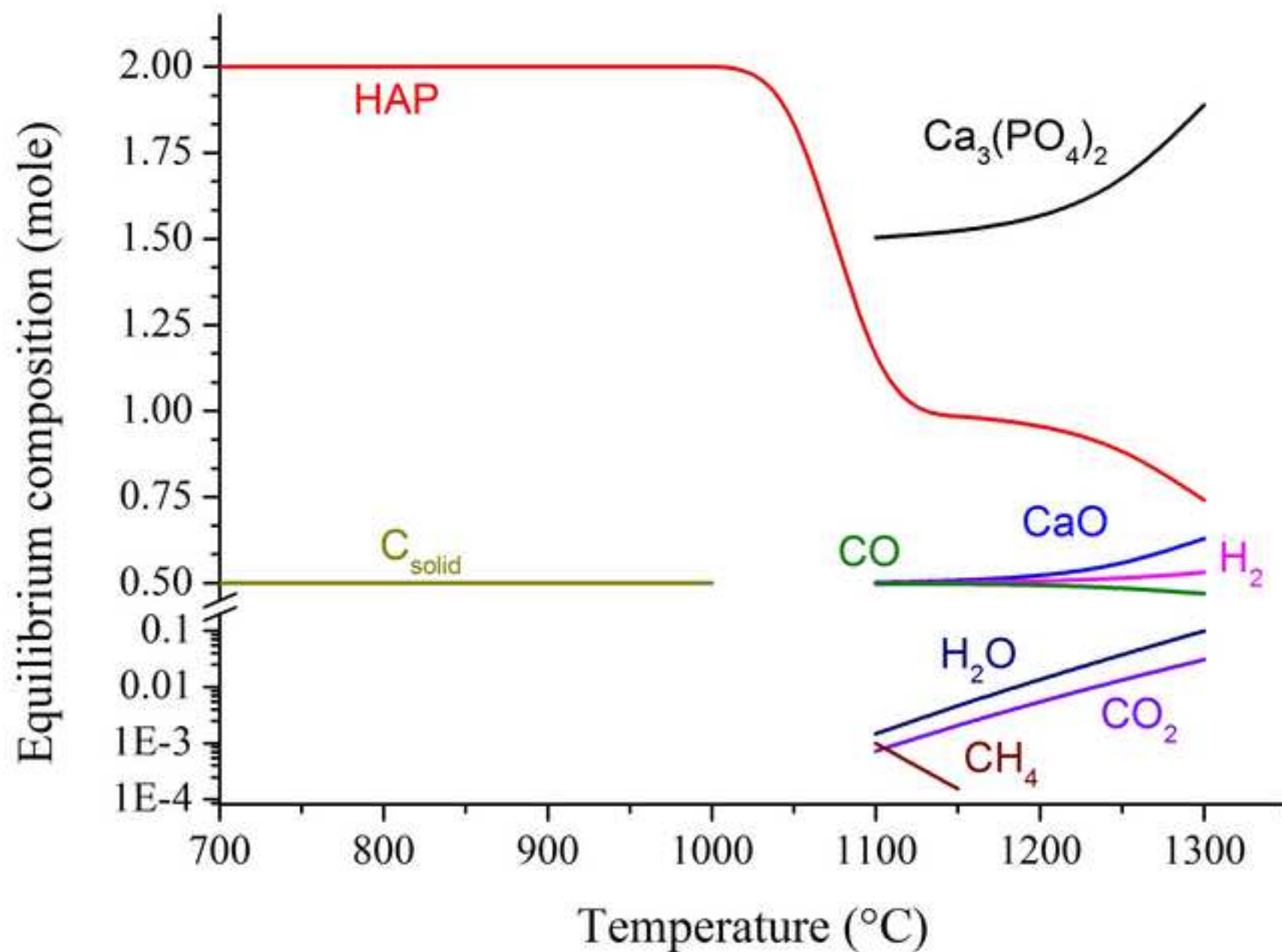


Figure2a

[Click here to download high resolution image](#)

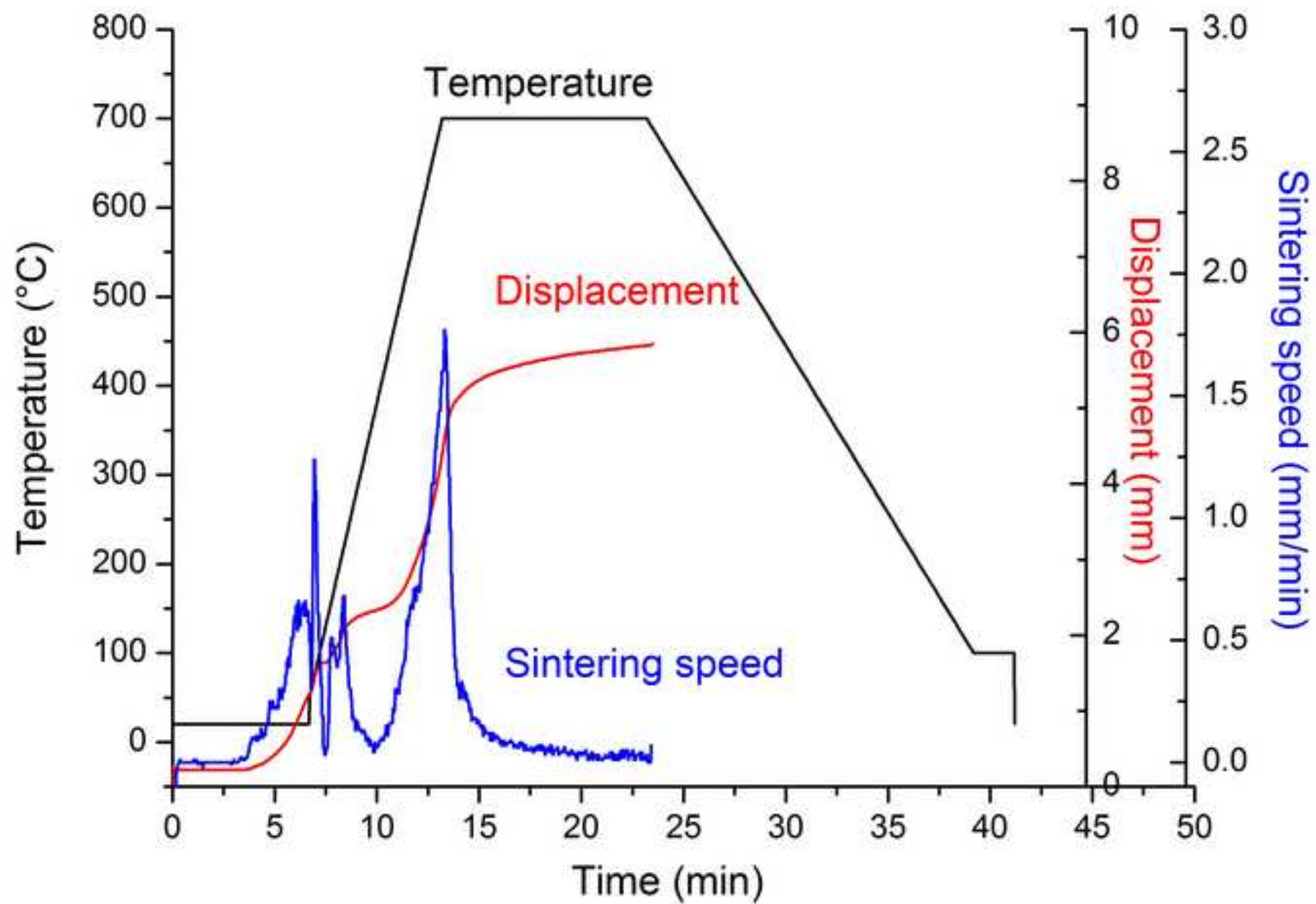


Figure2b

[Click here to download high resolution image](#)

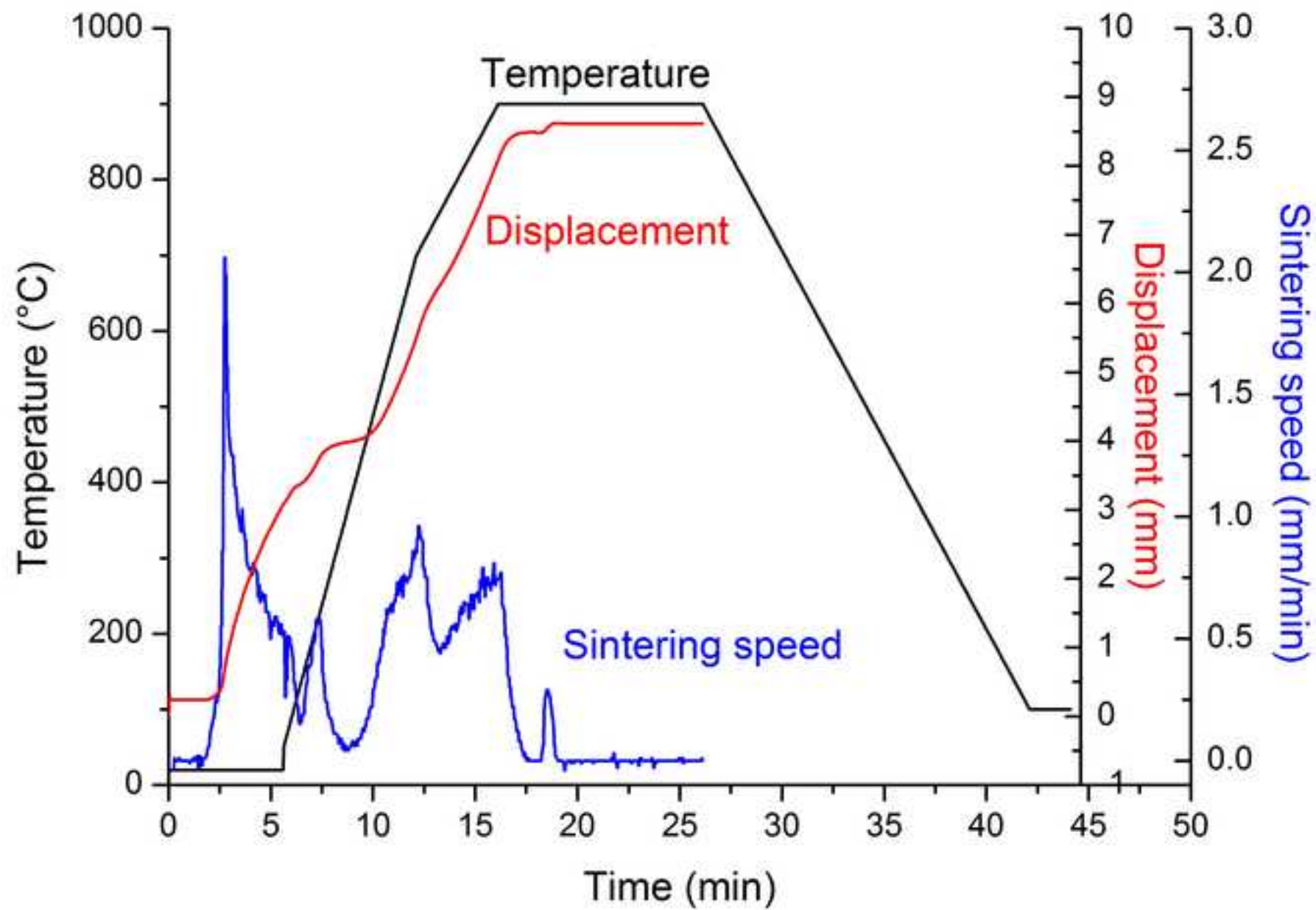


Figure3

[Click here to download high resolution image](#)

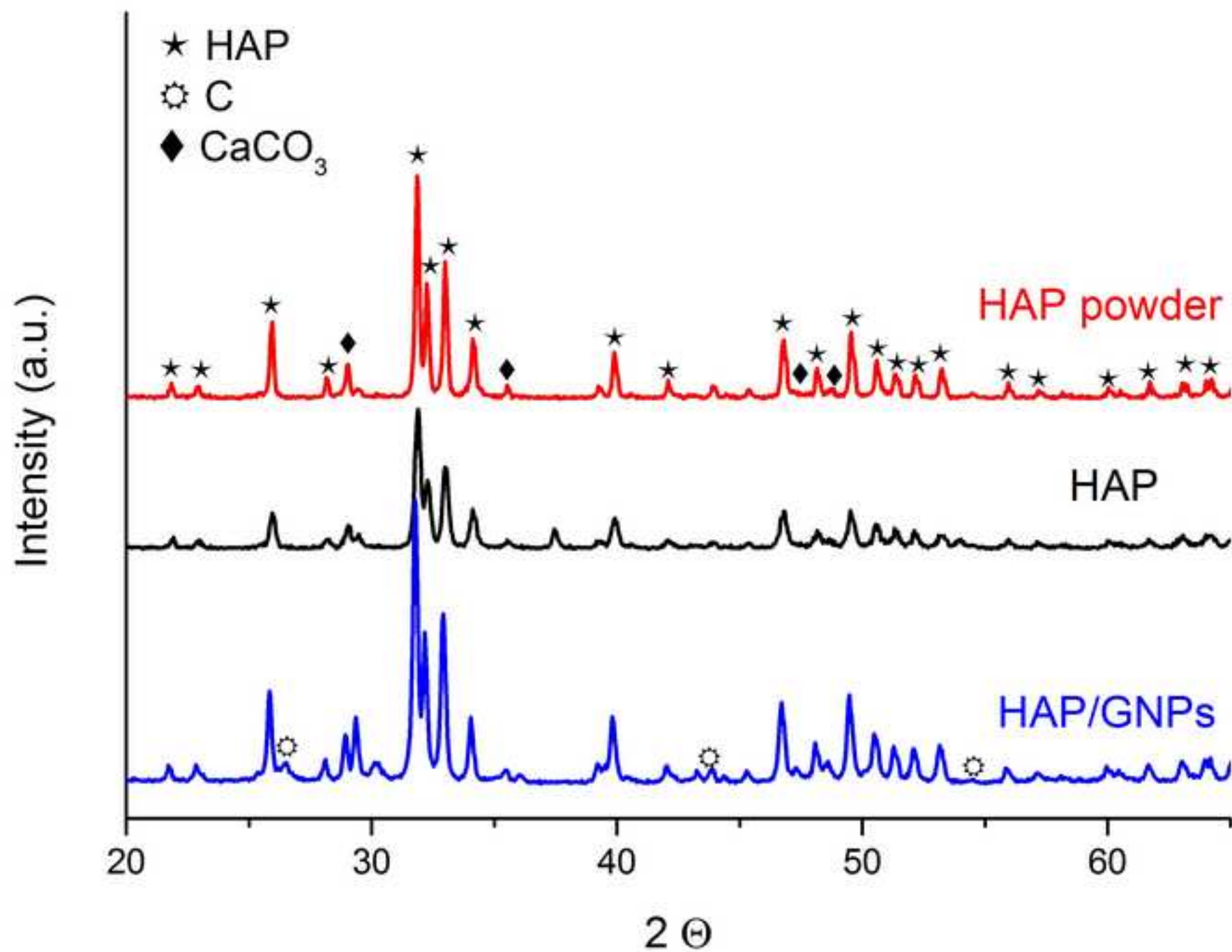




Figure4a

[Click here to download high resolution image](#)

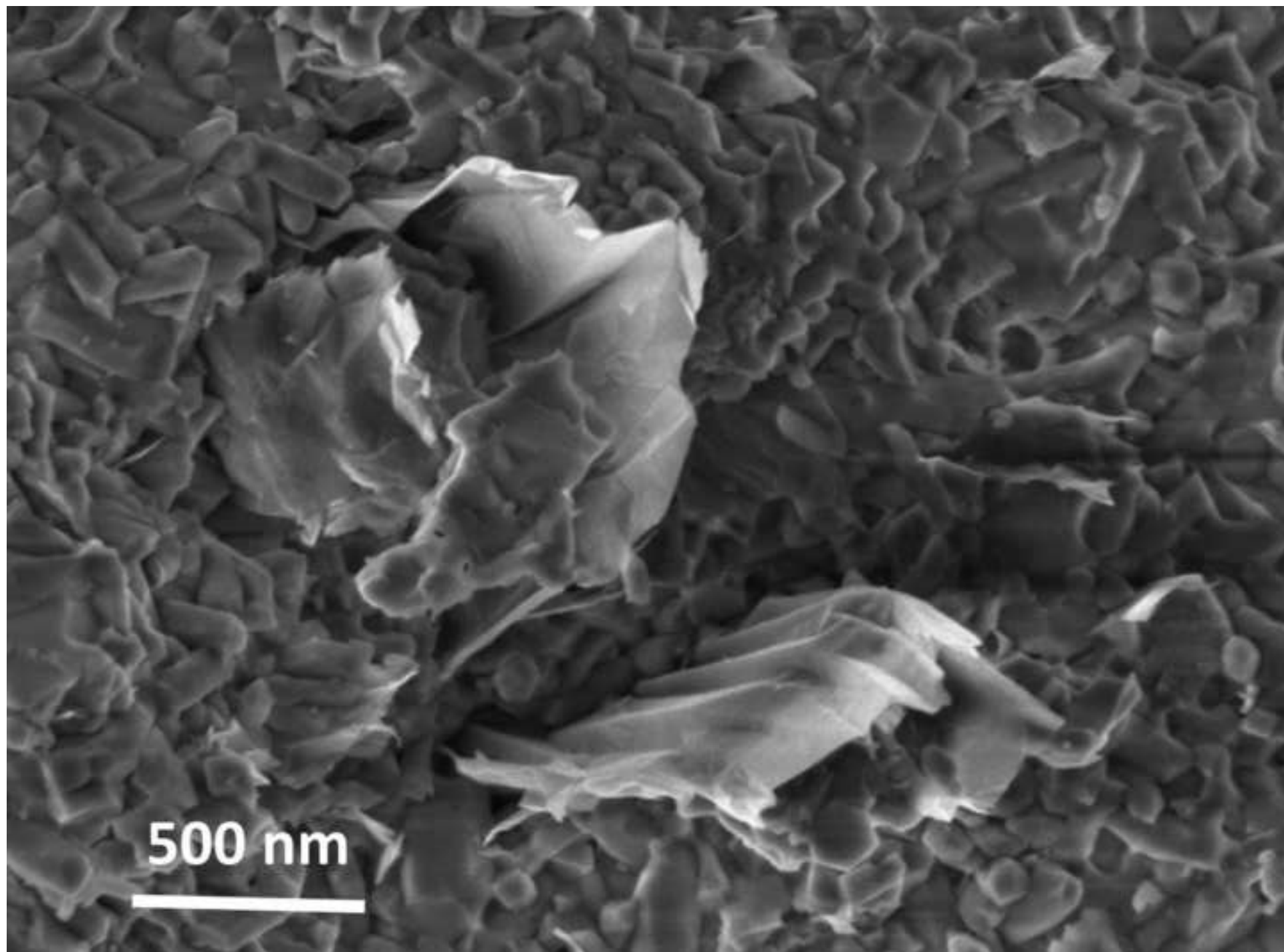




Figure4b  
[Click here to download high resolution image](#)

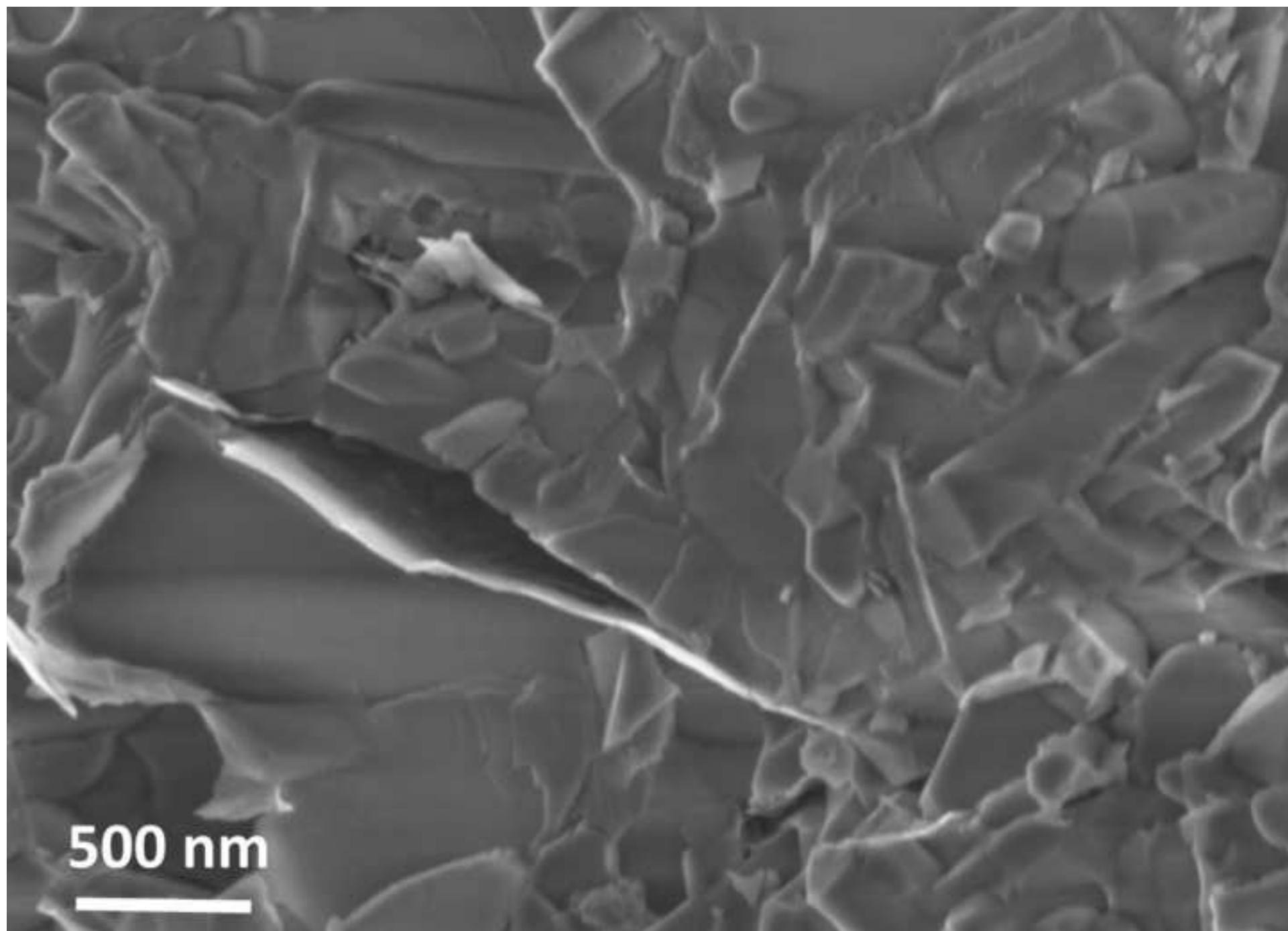


Figure4c

[Click here to download high resolution image](#)

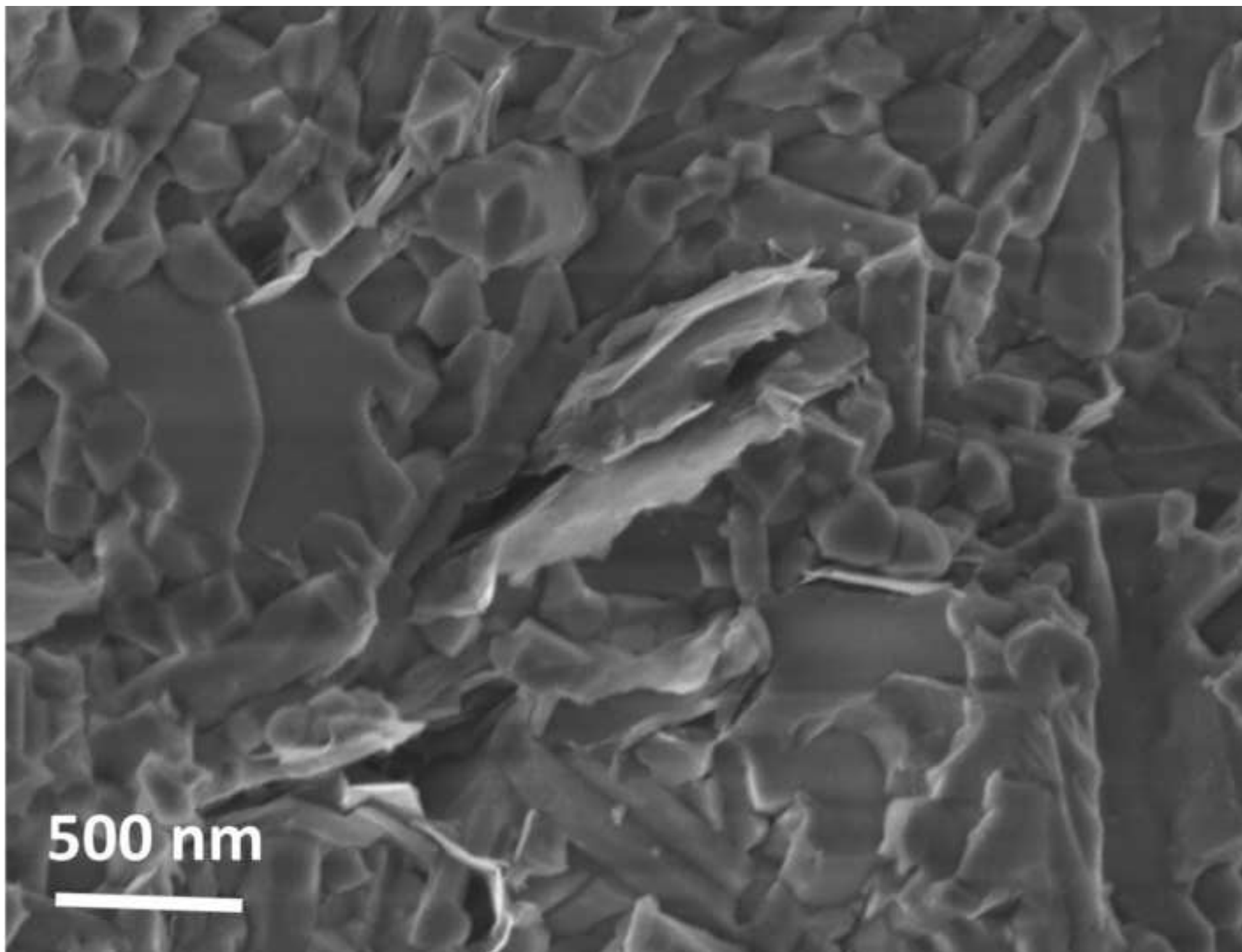
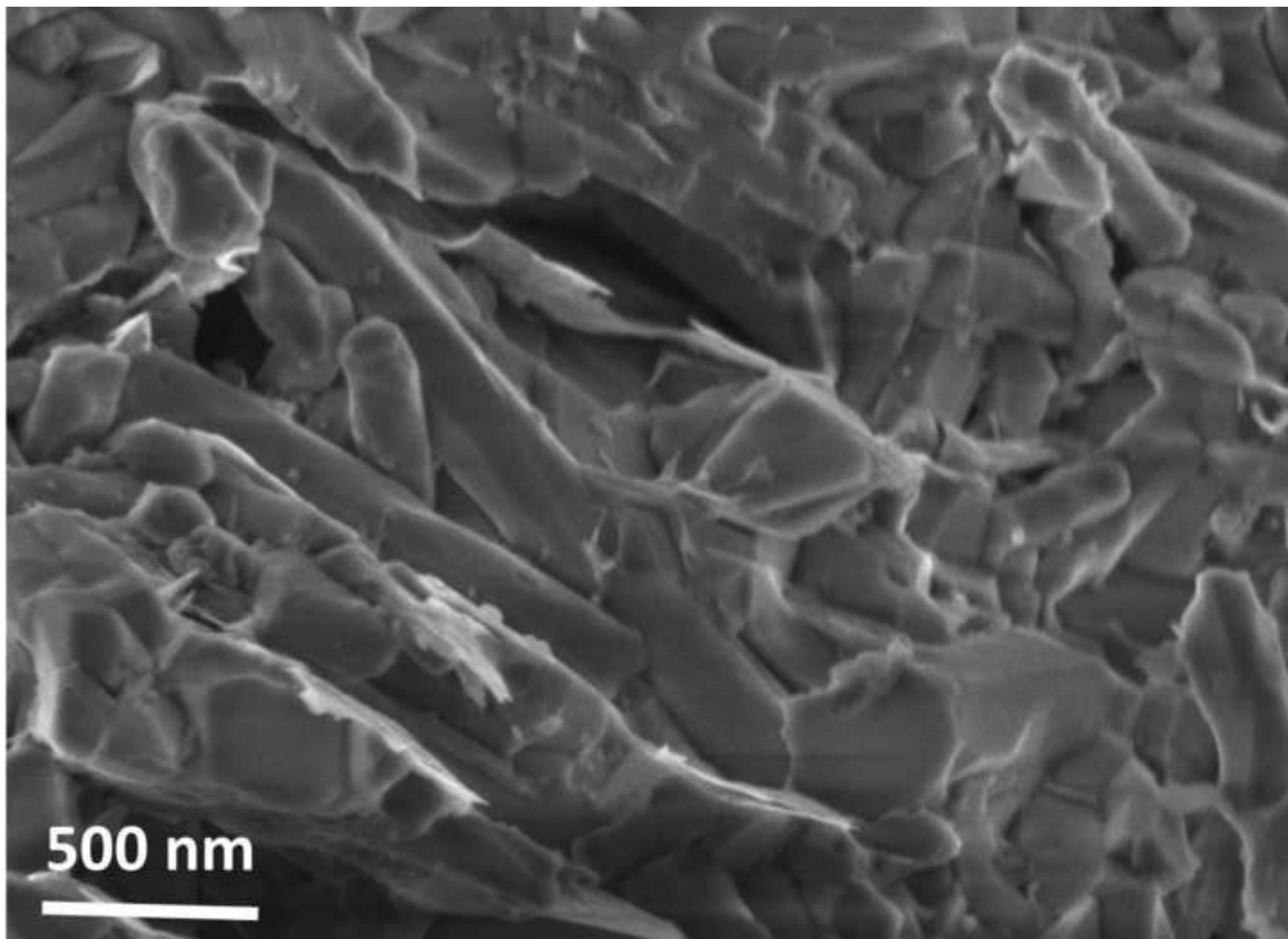


Figure4d  
[Click here to download high resolution image](#)



Sample	HAP wt%	GNPs wt%	SPS condition		
			Temperature [°C]	Pressure [MPa]	Time [min]
HG-5-7	98	2	700	30	5
HG-5-9			900		
HG-10-7			700		10
HG-10-9			900		

Table 1. SPS conditions during HAP composites preparation.

Sample	Composition of the synthesized powders (wt%) by XRD*			Relative density [%]	HV [GPa]	3 point bending strength [MPa]
	HAP	CaCO <sub>3</sub>	C			
HG-5-7	92	6	2	95.65	4 ± 0.5	119 ± 4.9
HG-10-7	92	6	2	95.88	3.5 ± 0.6	100 ± 4.8
HG-5-9	94	4	2	89.12	2.2 ± 0.4	84 ± 6.1
HG-10-9	94	4	2	87.44	2 ± 0.4	91± 5.2

Table 2. Characteristics and properties of the sintered samples